



This is the accepted manuscript made available via CHORUS. The article has been published as:

Finite-Temperature Hydrogen Adsorption and Desorption Thermodynamics Driven by Soft Vibration Modes

Sung-Jae Woo, Eui-Sup Lee, Mina Yoon, and Yong-Hyun Kim

Phys. Rev. Lett. **111**, 066102 — Published 5 August 2013

DOI: [10.1103/PhysRevLett.111.066102](https://doi.org/10.1103/PhysRevLett.111.066102)

Finite-Temperature Hydrogen Adsorption/Desorption Thermodynamics Driven by Soft Vibration Modes

Sung-Jae Woo,^{1,#} Eui-Sup Lee,^{1,#} Mina Yoon,² and Yong-Hyun Kim^{1,*}

¹*Graduate School of Nanoscience and Technology (WCU), KAIST, Daejeon 305-701,
Korea*

²*Center for Nanophase Materials Sciences, Oak Ridge National Laboratory, Oak Ridge,
TN 37831, U.S.A.*

[#]*These authors contributed equally.*

**Corresponding Author: yong.hyun.kim@kaist.ac.kr*

(Received: June 21, 2013)

Abstract

It has been widely accepted that enhanced dihydrogen adsorption is required for room-temperature hydrogen storage on nanostructured porous materials. Here we report, based on results of first-principles total energy and vibrational spectrum calculations, finite-temperature adsorption/desorption thermodynamics of hydrogen molecules that are adsorbed on the metal center of metallo-porphyrin incorporated graphene. We have revealed that the room-temperature hydrogen storage is achievable not only with the enhanced adsorption enthalpy, but also with soft-mode driven vibrational entropy of the adsorbed dihydrogen molecule. The soft vibration modes mostly result from multiple orbital coupling between the hydrogen molecule and the buckled metal center, for example, in Ca-porphyrin incorporated graphene. Our study suggests that the current design strategy for room-temperature hydrogen storage materials should be modified with explicitly taking the finite-temperature vibration thermodynamics into account.

Gas adsorption on nanostructured porous materials [1,2] is closely associated with a wide variety of energy conversion/storage physicochemical processes such as catalysis [3-5], greenhouse gas (for examples, CO₂ and NO) capture [6-8], and hydrogen storage [9-13]. The efficiency and cost of such renewable energy technologies operating at ambient conditions, however, are not satisfactory yet mostly because gaseous molecules interact either too weakly or too strongly with materials. It is generally believed that an optimal solution would be obtained with an intermediate binding strength of gas molecules, for examples, the volcanic curve in catalysis [14] and the Kubas interaction in hydrogen storage [10,11].

For room-temperature hydrogen storage, many have attempted theoretically [10-13,15-17] and experimentally [18,19] to design nanostructured materials with enhanced dihydrogen adsorption sites beyond the typical van der Waals interaction of < 0.1 eV per H₂. It has been widely accepted [10,11,15-17] that, in order to overcome the intrinsic fugacity of ambient H₂ gas (0.4 eV per H₂), one may need nanostructured materials with the H₂ adsorption energies of 0.2-0.6 eV per H₂. The target interaction range has been rather broad because of the ambiguity in the entropic contribution of the adsorbed H₂. For room-temperature H₂ storage, it was proposed that a binding strength of 0.15 eV per H₂ would be optimal for van der Waals type physisorption based on grand-canonical Monte Carlo simulations [20], whereas a binding strength of 0.3 eV per H₂ would be optimal for intermediate Kubas-type chemisorption based on grand-canonical partition function analyses for multi-H₂ adsorption per site with limitedly considering the zero-point vibration energy [16]. The precise finite-temperature H₂ adsorption/desorption thermodynamics with fully considering the entropy of weakly-adsorbed H₂ at the first-principles level has never been examined closely. In the experimental side [18,19], it has been difficult to increase the H₂ adsorption strength over 0.2 eV per H₂, and it is not clear if an enhanced dihydrogen adsorption energy of ~ 0.15 eV per H₂ would work for room-temperature hydrogen storage.

In this Letter, we report first-principles H_2 adsorption/desorption thermodynamics at finite temperature depending on various H_2 binding strengths from van der Waals to Kubas interactions on, as an example, metallo-porphyrin incorporated graphene systems [5,21-23]. We have found that enhanced dihydrogen adsorption is generally accompanied by an enhanced zero-point energy and a reduced entropic free-energy gain at finite temperature. A new strategy for designing room-temperature hydrogen storage materials is proposed; a nanostructured material is desirable with an intermediate H_2 binding strength of 0.15 eV and characteristic soft vibration modes less than 5 meV, as like Ca-porphyrin incorporated graphene.

Metallo-porphyrin incorporated graphene systems were first proposed theoretically [21] and later synthesized in experiment for Fe-porphyrin carbon nanotube [5]. Because the dihydrogen binding strength varies from van der Waals to Kubas types in theory, one can systematically examine finite-temperature hydrogen adsorption/desorption thermodynamics depending on the dihydrogen binding strength. We performed first-principles density function theory (DFT) total energy calculations for Zn-, Mg-, Ca-, Ti-, and V-porphyrin incorporated graphenes. We employed projector-augmented wave (PAW) potentials and Perdew-Burke-Ernzerhof (PBE) exchange-correlation functional [24], and selectively included the van der Waals (vdW) correction [25], as implemented in the Vienna Ab initio Simulation Package (VASP) [26]. It has been known that the *ad hoc* combination of PBE and vdW correction works well for vdW systems, whereas PBE alone does for Kubas systems at certain accuracy [27-29]. The (8×8) graphene supercell with a 20-Å vacuum space, the $(3\times 3\times 1)$ mesh for the \mathbf{k} -points integration, and the energy cutoff of 400 eV were used. For accurate calculations of vibrational spectra, we first tightly optimized the atomic forces less than 10^{-3} eV/Å, and then calculated dynamic matrices separately for an adsorbed H_2 with various vibrational displacements from 0.005 to 0.3 Å depending on softness of each

vibrational mode and metallo-porphyrin incorporated graphenes up to the (3x3) region with a fixed displacement of 0.02 Å. The soft vibration modes of the adsorbed H₂ were carefully double checked with potential energy surface calculations. In this way, we were able to completely avoid any spurious imaginary frequency that can otherwise appear readily for soft vibration modes because of numerical noises in typical plane-wave based DFT softwares.

Finite-temperature hydrogen adsorption/desorption thermodynamics on metallo-porphyrin incorporated graphenes (M-PIGs) can be cast into the variation of the Gibbs free energy at pressure P and temperature T [30],

$$\Delta G(T, P) = G_{\text{H}_2@\text{M-PIG}}(T, P) - G_{\text{M-PIG}}(T, P) - \mu_{\text{H}_2}(T, P), \quad (1)$$

where $G(T, P)$ represents the Gibbs free energy of a system,

$$G(T, P) = E + F_{\text{vib}}(T) + PV(T, P). \quad (2)$$

$\mu_{\text{H}_2}(T, P)$ is the chemical potential of H₂ gas,

$$\begin{aligned} \mu_{\text{H}_2}(T, P) &= E_{\text{H}_2} + \text{ZPE}_{\text{H}_2} + H^0(T) - H^0(0) - TS^0(T) + k_{\text{B}}T \ln \frac{P}{P_0} \\ &= E_{\text{H}_2} + \text{ZPE}_{\text{H}_2} + \mu_{\text{H}_2}^0(T) + k_{\text{B}}T \ln \frac{P}{P_0}. \end{aligned} \quad (3)$$

In Eqs. (2) and (3), E is the DFT total energy, ZPE is the zero-point energy ($= \sum \frac{\hbar\omega_i}{2}$), and $F_{\text{vib}}(T)$ is the vibrational Helmholtz free energy [30],

$$F_{\text{vib}}(T) \approx \sum_{i=1}^{3N} \left[\frac{\hbar\omega_i}{2} + k_{\text{B}}T \ln \left\{ 1 - \exp \left(-\frac{\hbar\omega_i}{k_{\text{B}}T} \right) \right\} \right], \quad (4)$$

where $\hbar\omega_i$ is the DFT-obtained vibrational energy of normal modes, k_{B} is the Boltzmann constant, and $3N$ is the total number of vibrational modes. The PV term in Eq. (2) is negligible for solid-state systems [30]. The temperature-dependent standard enthalpy H^0 and entropy S^0 of H₂ gas at standard pressure ($P_0 = 1$ bar) for $\mu_{\text{H}_2}^0(T) = H^0(T) - H^0(0) - TS^0(T)$ were taken from the thermochemical table [30,31,32] and fitted with polynomials.

Because vibrational normal modes are subjective to the H_2 adsorption strength (E_{ads}) through the causality, we can decompose ΔG into

$$\Delta G(T, P) = \Delta E + \Delta \text{ZPE} + \Delta F(T) - \mu_{H_2}^0(T) - k_B T \ln \frac{P}{P_0}, \quad (5)$$

from Eqs. (1)-(4). The internal energy variation is $\Delta E = E_{H_2@M\text{-}PIG} - E_{M\text{-}PIG} - E_{H_2}$, the ZPE variation is $\Delta \text{ZPE} = \text{ZPE}_{H_2@M\text{-}PIG} - \text{ZPE}_{M\text{-}PIG} - \text{ZPE}_{H_2}$, and $\Delta F(T)$ is the variation of the vibrational entropic free energy – the second term in the right hand side of Eq. (4). Note that both ΔZPE and ΔF in Eq. (5) sensitively depend on $\Delta E = -E_{\text{ads}}$, as discussed below.

We first calculated low-energy H_2 configurations weakly adsorbed on Zn-, Mg-, and Ca-PIGs with the vdW correction, obtaining adsorption energies of 0.078, 0.140, and 0.144 eV per H_2 , respectively. For Kubas-type V and Ti-PIGs, the H_2 adsorption energies are 0.232 and 0.339 eV per H_2 , respectively, without the vdW correction. Because the H_2 binding strength is almost evenly distributed from 0.08 to 0.34 eV, as summarized in Table I, we are ready to discuss E_{ads} -dependent ΔZPE and ΔF contributions to finite-temperature H_2 adsorption thermodynamics [33].

Figure 1 and Table II summarizes six characteristic vibrational normal modes and the calculated vibration frequencies, respectively, of H_2 on M-PIGs. The ZPE of a free H_2 is calculated to be 266 meV with the H-H stretching frequency of 532 meV, irrespective of the vdW correction. The total ZPEs of H_2 -M-PIGs slightly vary, depending on the vibration spectrum range included for M-PIG [see Fig. S1 in Ref. 34]. As an illustration, total and local vibrational spectra before and after H_2 adsorption on representative Zn- and Ti-PIGs are displayed in Fig. 2.

When the dihydrogen interaction is weak as in vdW-corrected systems (Zn-, Mg-, and Ca-PIGs), the H-H stretching mode as shown in Fig. 1(a) slightly downshifts by <10 meV, and five soft vibration modes are generated within the range of 100 meV (see Fig. 2 and Table II).

Consequently, the total ZPEs increase upon the adsorption of H_2 , which hinders the H_2 adsorption. When the Kubas chemical coupling is prominently involved as for V- and Ti-PIGs, the H-H stretching mode downshifts noticeably more than 100 meV, and the five soft vibration modes distribute from tens to a few hundreds meV in vibrational energy (see Table II and Fig. 2). In this case, ΔZPE is more than 100 meV, as listed in Table I. Figure 3(a) clearly shows that ΔZPE is generally proportional to the H_2 binding strength. Specifically, ΔZPE is about 50% of E_{ads} for weakly interacting systems, but it is rather constant at around 0.12 eV per H_2 for strongly coupled systems. Although the trend is only based on five examples, it is clear that ΔZPE behaves differently from the rough estimation of $\Delta ZPE = 0.25E_{\text{ads}}$ in the literature [16].

The finite-temperature vibrational entropic free-energy variation ΔF is sensitively subjective to low-energy frequencies, according to the second term in the right hand side of Eq. (4). When $\hbar\omega_i \ll k_B T$, ΔF in Eq. (5) diverges negatively. For weakly-interacting Zn- and Ca-PIGs with low-energy soft vibration modes less than 5 meV, ΔF is around -0.14 eV at $T = 300$ K. This largely surpasses ΔZPE , as shown in Figs. 3(a) and 3(b). The entropic free energy gain ΔF for Mg-PIG is only a half (-0.07 eV) for Ca-PIG despite the similar adsorption strength. This is because there is no soft vibration mode less than 5 meV for Mg-PIG. For strongly-coupled Kubas systems, $\Delta F(300 \text{ K})$ is as small as -0.03 eV, contributing negligibly to the adsorption thermodynamics. The entropic free energy of H_2 gas at room temperature should thus be solely overcome by the H_2 adsorption strength for strongly-coupled Kubas dihydrogen systems.

The finite-temperature H_2 adsorption/desorption thermodynamics was examined by plotting P - T phase diagrams for M-PIG systems, as shown in Fig. 4. The phase boundary between adsorbed and desorbed states was obtained by solving $\Delta G = 0$ in Eq. (5). This is equivalent to the grand canonical partition function approach with single adsorption site [16].

To contrast the effect of the vibration entropy, we displayed P - T diagrams with $\Delta F = 0$ and $\Delta F \neq 0$, respectively, in Fig. 4(a) and 4(b); one can clearly see that the vibration entropy of adsorbed H_2 plays a critical role in finite-temperature H_2 adsorption/desorption dynamics. The hydrogen adsorption/desorption at 300 K in Ca-PIG can be controlled with a pressure < 100 bar, only because of the soft vibration modes less than 5 meV. On the contrary, Mg-PIG with a similar H_2 adsorption strength requires a high pressure > 1000 bar for room-temperature H_2 storage, simply because of no soft mode less than 5 meV. We have found that, particularly, the frustrated in-plane translation modes, FT_x and FT_y as shown in Fig. 1(e) and 1(f), are soft and thus play a big role in finite-temperature H_2 adsorption/desorption thermodynamics; for Ca-PIG, their vibration energies are at 5.2 meV (FT_x) and 2.2 meV (FT_y). The difference in the vibrational energies of the FT modes for Ca- and Mg-PIGs can be attributed to the buckling behavior of the Ca and Mg atoms, as listed in Table I; because of the buckling, the H_2 σ orbital could couple similarly with multiple Ca $3d$ orbitals when H_2 is translated, and thus the energy surface becomes rather flat, generating soft modes [see Fig. S2 in Ref. 34]. This is not the case for the un-buckled Mg-PIG.

For strongly-coupled Kubas systems, the finite-temperature adsorption/desorption thermodynamics is less sensitive to ΔF than it is for weakly-coupled systems. Figure 4 strongly implies that in this case a precise control of the H_2 adsorption strength around 0.35 eV per H_2 is required for room-temperature H_2 storage with a pressure control < 100 bar. If the binding strength is too small as 0.25 eV per H_2 as in V-PIG, one needs to apply a high pressure > 1000 bar to store H_2 at 300 K. If it is too big as ~ 0.45 eV per H_2 , it would be too hard to desorb H_2 at 1 bar and 300 K, as implied by the stiff adsorption/desorption boundaries of V- and Ti-PIGs in Fig. 4. When we assume $\Delta E = -0.45$ eV for H_2 on Ti-PIG with the same vibration spectrum, H_2 desorption would occur at a pressure < 1 bar, as indicated by the phase diagram of Ti*-PIG in Fig. 4.

In conclusion, we have investigated finite-temperature thermodynamics of H_2 adsorbed on metallo-porphyrin incorporated graphenes with various binding strengths and vibration spectra, based on the first-principles density functional theory calculations. We found that the zero-point energy cancellation increases as the H_2 binding strength increases. On contrary, the soft vibration-mode driven entropic free energy gain decreases as the binding strength increases. An optimal adsorption mechanism for room temperature hydrogen storage is implied: a Kubas-type weak interaction of ~ 0.15 eV per H_2 with some soft vibration modes as like H_2 on Ca-porphyrin graphene or a typical Kubas interaction of ~ 0.34 eV per H_2 as like H_2 on Ti-porphyrin graphene. Following the generality of the vibrational Helmholtz free energy in Eq. (4) [30,32], we believe that the soft vibration-dominant finite-temperature thermodynamics would be generally applicable for many energy conversion/storage physicochemical processes associated with ambient gas adsorption [1,2].

Acknowledgement

We thank J. Kang and Y. Ihm for reading the manuscript. This work was supported by the WCU (R31-2008-000-10071-0), NRF (2012-046191), and Global Frontier R&D (2011-0031566: Center for Multiscale Energy Systems) programs funded by the Korea government (MEST). M.Y. was supported by the Materials Sciences and Engineering Division, Office of Basic Energy Sciences, U.S. Department of Energy, and the theme research at the Center for Nanophase Materials Sciences, which is sponsored at Oak Ridge National Laboratory by the Scientific User Facilities Division, Office of Basic Energy Sciences, U.S. Department of Energy.

References

- [1] J. F. Weaver, *Science* **339**, 39 (2013).
- [2] C. T. Campbell, J. R. V. Sellers, *J. Am. Chem. Soc.* **134**, 18109 (2012).
- [3] J. K. Nørskov, T. Bligaard, J. Rossmeisl, and C. H. Christensen, *Nat. Chem.* **1**, 37 (2009).
- [4] I. X. Green, W. Tang, M. Neurock, and J. T. Yates Jr., *Science* **333**, 736 (2011).
- [5] D. H. Lee, W. J. Lee, W. J. Lee, S. O. Kim, and Y.-H. Kim, *Phys. Rev. Lett.* **106**, 175502 (2011).
- [6] R. Vaidhyanathan, S. S. Iremonger, G. K. H. Shimizu, P. G. Boyd, S. Alavi, and T. K. Woo, *Science* **330**, 650 (2010).
- [7] J.-R. Li, Y. Ma, M. C. McCarthy, J. Sculley, J. Yu, H.-K. Jeong, P. B. Balbuena, and H.-C. Zhou, *Coord. Chem. Rev.* **255**, 1791 (2011).
- [8] H. Choi, Y. C. Park, Y.-H. Kim, and Y. S. Lee, *J. Am. Chem. Soc.* **133**, 2084 (2011).
- [9] L. Schlapbach and A. Züttel, *Nature* **414**, 353 (2001).
- [10] Y. Zhao, Y.-H. Kim, A. C. Dillon, M.J. Heben, and S. B. Zhang, *Phys. Rev. Lett.* **94**, 155504 (2005).
- [11] Y.-H. Kim, Y. Zhao, A. Williamson, M. J. Heben, and S. B. Zhang, *Phys. Rev. Lett.* **96**, 016102 (2006).
- [12] K. Lee, Y.-H. Kim, Y. Y. Sun, D. West, Y. Zhao, Z. Chen, and S. B. Zhang, *Phys. Rev. Lett.* **104**, 236101 (2010).
- [13] Y.-H. Kim, J. Kang, and S.-H. Wei, *Phys. Rev. Lett.* **105**, 236105 (2010).
- [14] J. K. Nørskov, J. Rossmeisl, A. Logadottir, L. Lindqvist, J. R. Kitchin, T. Bligaard, and H. Jonsson, *J. Phys. Chem. B* **108**, 17886 (2004).
- [15] E. Durgun, S. Ciraci, W. Zhou, and T. Yildirim, *Phys. Rev. Lett.* **97**, 226102 (2006).

- [16] H. Lee, W. I. Choi, and J. Ihm, Phys. Rev. Lett. **97**, 056104 (2006).
- [17] M. Yoon, S. Yang, C. Hicke, E. Wang, D. Geohegan, and Z. Zhang, Phys. Rev. Lett. **100**, 206806 (2008).
- [18] M. Dinca, A. Dailly, Y. Liu, C. M. Brown, D. A. Neumann, and J. R. Long, J. Am. Chem. Soc. **128**, 16876 (2006).
- [19] K. Sumida, D. Stuck, L. Mino, J.-D. Chai, E. D. Bloch, O. Zavorotynska, L. J. Murray, M. Dinca, S. Chavan, S. Bordiga, M. Head-Gordon, and J. R. Long, J. Am. Chem. Soc. **135**, 1083 (2013).
- [20] S. K. Bhatia and A. L. Myers, Langmuir **22**, 1688 (2006).
- [21] W. I. Choi, S.-H. Jhi, K. Kim, and Y.-H. Kim, Phys. Rev. B **81**, 085441 (2010).
- [22] Y.-H. Kim, Y. Y. Sun, W. I. Choi, J. Kang, and S. B. Zhang, Phys. Chem. Chem. Phys. **11**, 11400 (2009).
- [23] A. T. Lee, J. Kang, S.-H. Wei, K. J. Chang, and Y.-H. Kim, Phys. Rev. B **86**, 165403 (2012).
- [24] J. P. Perdew, K. Burke, and M. Ernzerhof, Phys. Rev. Lett. **77**, 3865 (1996).
- [25] S. Grimme, J. Comput. Chem. **27**, 1787 (2006).
- [26] G. Kresse and D. Joubert, Phys. Rev. B **59**, 1758 (1999).
- [27] Y. Y. Sun, K. Lee, Y.-H. Kim, and S. B. Zhang, Appl. Phys. Lett. **95**, 033109 (2009).
- [28] Y. Ohk, Y.-H. Kim, and Y. Jung, Phys. Rev. Lett. **104**, 179601 (2010).
- [29] Y. Y. Sun, K. Lee, L. Wang, Y.-H. Kim, W. Chen, Z. Chen, and S. B. Zhang, Phys. Rev. B **82**, 073401 (2010).
- [30] K. Reuter and M. Scheffler, Phys. Rev. B **65**, 035406 (2002).
- [31] M. W. Chase *et al.*, J. Phys. Chem. Ref. Data **14**, 927 (1985).
- [32] M. Yoon, H. H. Weitering, and Z. Zhang, Phys. Rev. B **83**, 045413 (2011).

[33] Calculated adsorption energies and metal-H₂ distances in Table I indicate that a Kubas-type H₂ interaction is commonly associated for Mg-, Ca-, Ti-, and V-PIGs [13], but a vdW-type H₂ interaction is for Zn-PIG.

[34] Supplemental Materials: Figure S1 and Figure S2.

TABLE I. DFT-calculated hydrogen adsorption energy (E_{ads}), metal- H_2 separation (d), metal-graphene separation (Δz), and zero point energy correction (ΔZPE) for H_2 -adsorbed metallo-porphyrin incorporated graphenes.

	Zn	Mg	Ca	V	Ti
E_{ads} (eV)	0.078	0.140	0.144	0.232	0.339
d (Å)	2.763	2.439	2.666	1.849	1.876
Δz (Å)	0.04	0.25	1.46	0.78	0.85
ΔZPE (eV)	0.048	0.080	0.067	0.120	0.118

TABLE II. DFT-calculated vibration energy (in the unit of meV) of H_2 -related normal modes on metallo-porphyrin incorporated graphenes. The number in parenthesis is the vibrational perturbation displacement (in the unit of Å) used in computation. The normal vibration modes consist of H-H stretching motion ($\omega_{\text{H-H}}$), frustrated rotations (VO_{out} , and FR_z) and frustrated translations (VO_{in} , FT_x , and FT_y), as shown in Fig. 1. The ZPE (in the unit of meV) is also listed. $\omega_{\text{H-H}}$ of free H_2 is 532 meV.

	$\omega_{\text{H-H}}$	VO_{out}	VO_{in}	FR_z	FT_x	FT_y	ZPE
Zn	531.093 (0.020)	36.601 (0.020)	31.040 (0.020)	12.862 (0.020)	10.460 (0.100)	3.254 (0.040)	312.655
Mg	525.677 (0.005)	75.237 (0.005)	46.632 (0.005)	17.602 (0.005)	13.184 (0.030)	8.890 (0.030)	343.611
Ca	527.148 (0.005)	69.464 (0.005)	45.971 (0.005)	15.249 (0.005)	5.180 (0.080)	2.210 (0.200)	332.612
V	409.194 (0.005)	157.933 (0.005)	106.464 (0.005)	39.271 (0.005)	14.601 (0.300)	23.270 (0.060)	375.367
Ti	358.700 (0.005)	166.566 (0.005)	97.199 (0.005)	81.121 (0.005)	24.656 (0.020)	33.076 (0.020)	380.659

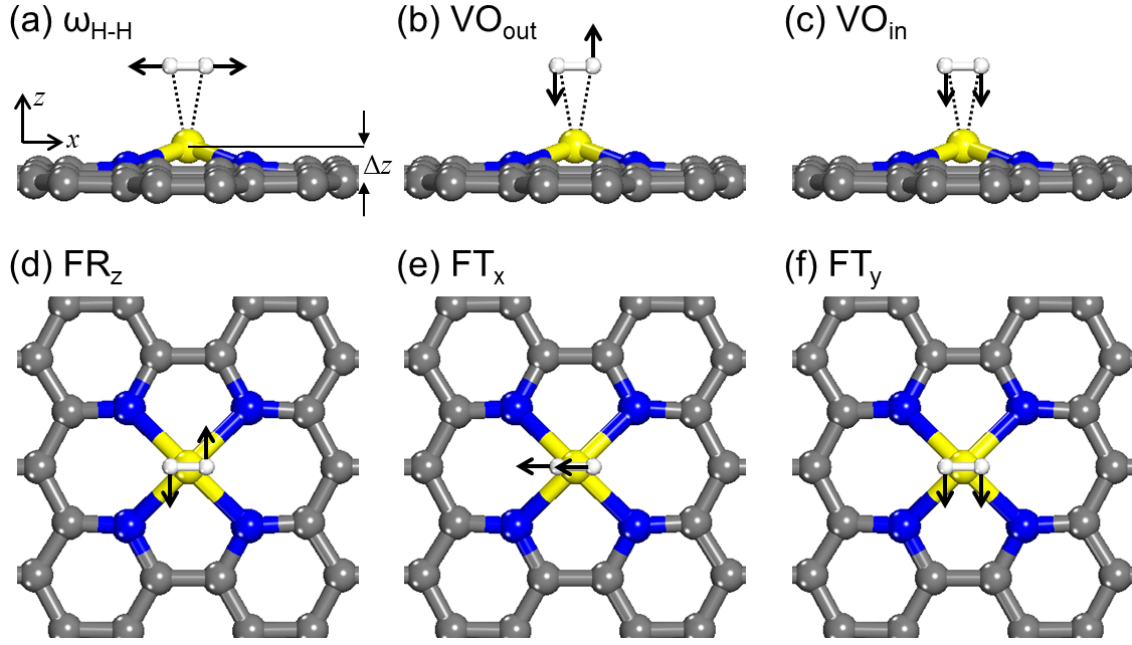


FIG. 1 (Color online). Six vibrational normal modes (marked by arrows) of a H_2 molecule adsorbed onto a metallo-porphyrin incorporated graphene: (a) H-H bond stretching mode ($\omega_{\text{H-H}}$), (b) vertical out-of-phase oscillation (VO_{out}), (c) vertical in-phase oscillations (VO_{in}), (d) frustrated rotation along the z axis (FR_z), (e) frustrated translation in the x direction (FT_x), and (f) frustrated translation in the y direction (FT_y). The buckled distance (Δz) of metal atom from graphene plane in (a) is listed in Table I.

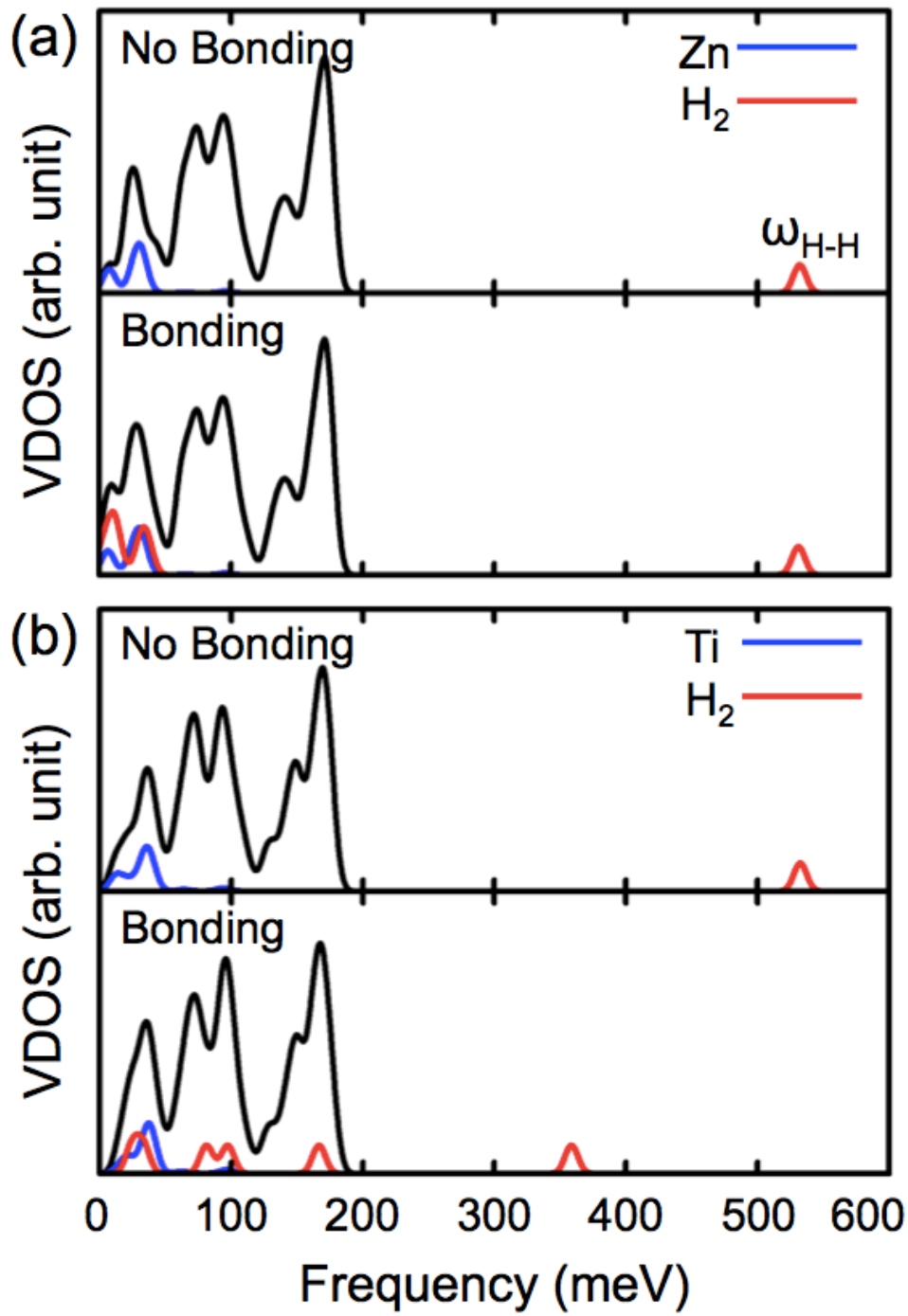


FIG. 2 (Color online). Vibrational density of states (VDOS) before and after H_2 adsorption on (a) Zn-PIG and (b) Ti-PIG. Local VDOS are depicted for the metal center and H_2 molecule. The H-H bond stretching mode is marked with ω_{H-H} .

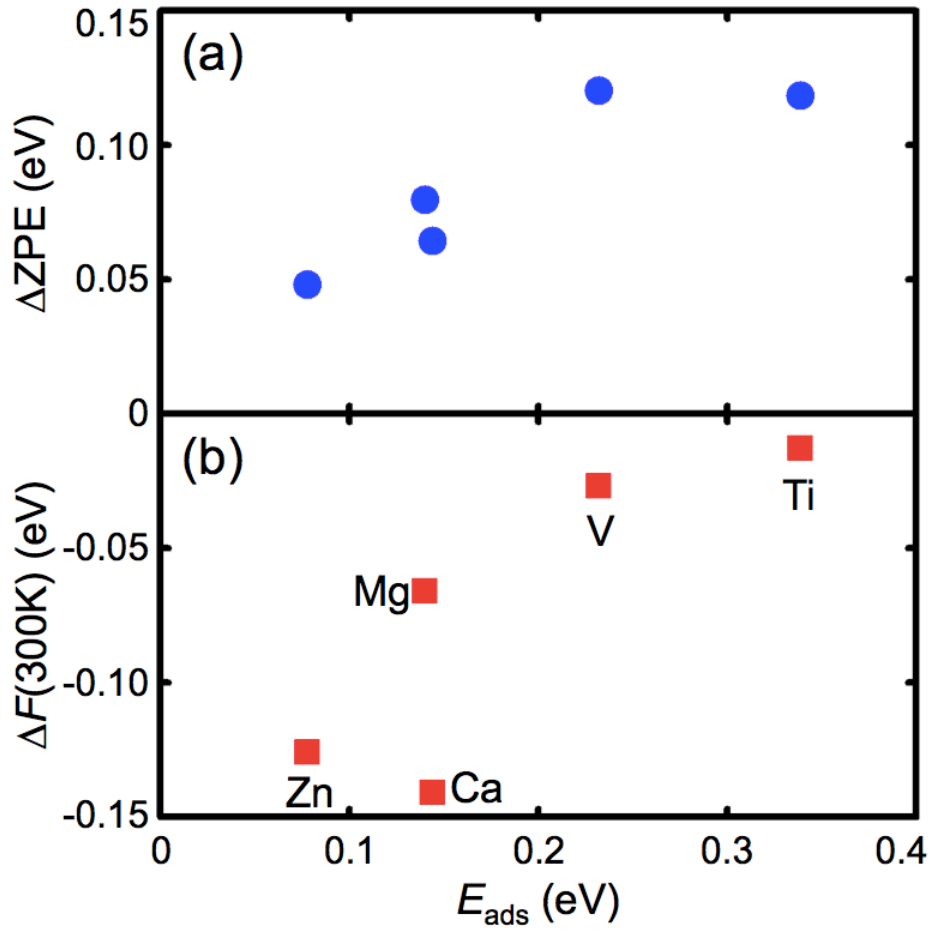


FIG. 3 (Color online). (a) Zero-point energy variation (ΔZPE) and (b) vibrational entropic free energy variation (ΔF) at $T = 300$ K as a function of H₂ adsorption energy (E_{ads}).

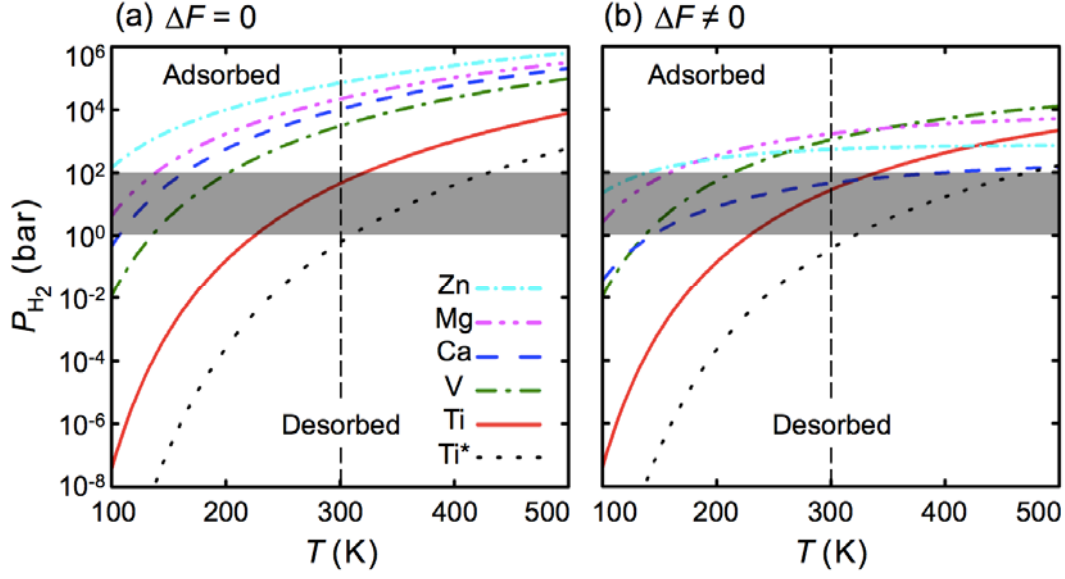


FIG. 4 (Color online). H_2 adsorption/desorption P - T phase diagram on metallo-porphyrin incorporated graphenes (a) without and (b) with considering the vibrational entropic free energy variation ΔF . A H_2 phase diagram of a virtual Ti^* -PIG system was simulated, in which $\Delta E = -0.45$ eV with the same vibration spectrum with Ti -PIG.